![The University of Osaka Institutional Knowledge Archive OUKA logo]

The University of Osaka
Institutional Knowledge Archive

Title	Destabilization of nonlinear resistive wall mode due to suppression of poloidal rotation in a cylindrical tokamak
Author(s)	Sato, M.; Hamaguchi, S.; Wakatani, M.
Citation	Physics of Plasmas. 2003, 10(1), p. 187-194
Version Type	VoR
URL	https://hdl.handle.net/11094/78489
rights	This article may be downloaded for personal use only. Any other use requires prior permission of the author and AIP Publishing. This article appeared in Physics of Plasmas 10, 187 (2003) and may be found at https://doi.org/10.1063/1.1527042.
Note	

Destabilization of nonlinear resistive wall mode due to suppression of poloidal rotation in a cylindrical tokamak

M. Sato, S. Hamaguchi, and M. Wakatani

View Online   Export Citation

ARTICLES YOU MAY BE INTERESTED IN

Nonlinear evolution of resistive wall mode in a cylindrical tokamak with poloidal rotation
Physics of Plasmas **13**, 102507 (2006); https://doi.org/10.1063/1.2358965

Resistive wall mode stabilization with internal feedback coils in DIII-D
Physics of Plasmas **11**, 2505 (2004); https://doi.org/10.1063/1.1666238

What is a stellarator?
Physics of Plasmas **5**, 1647 (1998); https://doi.org/10.1063/1.872833
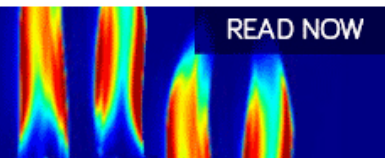
Destabilization of nonlinear resistive wall mode due to suppression of poloidal rotation in a cylindrical tokamak

M. Sato, S. Hamaguchi, and M. Wakatani
Graduate School of Energy Science, Kyoto University, Gokasho, Uji 611-1100, Japan

It is known that linear resistive wall modes (RWMs) can be stabilized by a poloidal rigid rotation. Nonlinear behavior of unstable RWMs has been studied in a cylindrical tokamak plasma with such a poloidal rotation. When a resistive wall is very close to the plasma surface ($r_w/a \simeq 1.2$) significant reduction of the poloidal rotation due to the Maxwell stress occurs in the neighborhood of resonant surface of $(m,n)=(2,1)$, where m (n) is a poloidal (toroidal) mode number. Thus the nonlinear saturated state does not depend on the magnitude of poloidal rotation. However, when the resistive wall position is close to the ideal wall stabilization limit ($r_w/a = 1.3$) or $r_w/a \simeq 1.27$, the poloidal rotation remains in the nonlinear phase for a large poloidal rotation case. In this case, nonlinear saturation with a small amplitude level becomes possible. The role of Maxwell stress is clarified by introducing magnetic island width and rotational torque for the reduction of poloidal rotation. © *2003 American Institute of Physics.* [DOI: 10.1063/1.1527042]

I. INTRODUCTION

Magnetohydrodynamic (MHD) stability of magnetically confined plasmas is crucial for obtaining improved confinement suitable for a fusion reactor.[1] For obtaining high beta plasmas, stabilization of dangerous ideal kink modes is required in current carrying tokamaks.[2] The ideal kink modes can be stabilized by a perfect conducting wall placed sufficiently close to the plasma surface.[3] However, when the wall has a finite conductivity, the mode cannot be stabilized completely, even if the wall is close to the plasma surface.[4] In this situation, resistive wall modes (RWMs) become unstable. The RWM grows slowly with a growth time on the order of resistive decay time of magnetic field, τ_w, in a wall. For a stationary tokamak sustained with a large bootstrap current, such a slowly growing instability becomes dangerous and it is important to stabilize RWMs. There are several experimental results that the RWMs deteriorate confinement in tokamaks.[5–7] For suppressing effects due to RWMs feedback controls have been proposed.[8,9]

It is noted that the linear RWMs can be stabilized by plasma rotation.[10–14] Indeed, in DIII-D tokamak, high beta plasmas with $\beta_N > \beta_N^{\text{no wall}}$ are obtained for sufficiently longer times than τ_w when the toroidal rotation is sufficiently fast.[7] Here, β_N is a normalized beta with respect to Troyon limit and $\beta_N^{\text{no wall}}$ is the β_N limit predicted under the assumption without a conducting wall.

However, when the plasma rotation decreases below a critical level, the RWM begins to grow as shown in the experiment.[7] As the RWM grows, the plasma rotation frequency decreases clearly. Finally, the high beta plasma phase of discharge is destroyed.

It is considered that the slowdown of plasma rotation results from the electromagnetic drag force.[15] Nave and Wesson showed that the electromagnetic drag force comes from perturbed magnetic fields penetrating into the resistive wall. Here we show that the magnetic perturbation due to the

RWM has a role to suppress the poloidal rotation through the Maxwell stress. The resultant slowdown of plasma rotation significantly affects stability of RWMs and their nonlinear behavior.

In this paper, we study numerically nonlinear behavior of RWMs in a cylindrical plasma with a rigid poloidal rotation. This may be a simplified model for understanding nonlinear physics of RWMs applicable to those in tokamak experiments. The rest of the paper is organized as follows. In Sec. II, for describing nonlinear RWMs in the cylindrical geometry, the reduced MHD equations are introduced. Then our numerical model for studying nonlinear RWMs are shown. Numerical schemes for solving the reduced MHD equations are briefly mentioned. In Sec. III, results of nonlinear calculations of unstable RWMs are shown. Our concern is in the change of the assumed poloidal rotation due to the nonlinear RWM with $(m,n)=(2,1)$, where m (n) is a poloidal) mode number. Finally, a summary is given in Sec. IV.

II. MODELING OF RWM

For low beta cylindrical tokamak plasmas, the well-known reduced MHD equations were derived by Kadomtsev and Pogutse[16] and Strauss.[17] These equations with dimensionless variables are shown as

$$\frac{\partial \psi}{\partial t} = \frac{\partial \phi}{\partial r}\frac{1}{r}\frac{\partial \psi}{\partial \theta} - \frac{1}{r}\frac{\partial \phi}{\partial \theta}\frac{\partial \psi}{\partial r} - \frac{\partial \phi}{\partial \zeta} + \eta J_\zeta - E_\zeta, \quad (1)$$

$$\frac{\partial U}{\partial t} = \frac{\partial \phi}{\partial r}\frac{1}{r}\frac{\partial U}{\partial \theta} - \frac{1}{r}\frac{\partial \phi}{\partial \theta}\frac{\partial U}{\partial r} + \frac{\partial J_\zeta}{\partial r}\frac{1}{r}\frac{\partial \psi}{\partial \theta} - \frac{1}{r}\frac{\partial J_\zeta}{\partial \theta}\frac{\partial \psi}{\partial r}$$

$$- \frac{\partial J_\zeta}{\partial \zeta} + \nu \nabla_\perp^2 U + S_m, \quad (2)$$

$$J_\zeta = \nabla_\perp^2 \psi, \quad (3)$$

$$U = \nabla_\perp^2 \phi, \qquad (4)$$

in the cylindrical coordinates (r, θ, ζ), where ψ is the poloidal magnetic flux defined by $\mathbf{B}_\perp = -(a/R)\nabla\psi\times\mathbf{e}_\zeta$ and ϕ is the stream function defined by $\mathbf{v}_\perp = \nabla\phi\times\mathbf{e}_\zeta$. Here, r, θ and ζ are radial, poloidal and toroidal coordinate, respectively. In Eq. (1), resistivity η is normalized to $\mu_0 a^2/\tau_{hp}$, where $\tau_{hp} = R\sqrt{\mu_0\rho}/B_0$. Here, the length of cylindrical plasma is $2\pi R$, the plasma minor radius is a, the mass density is ρ, and the longitudinal magnetic field is B_0. In Eq. (2), viscosity is denoted by ν. The source term S_m is chosen to satisfy $\nu\nabla_\perp^2 U_{eq}(r) + S_m = 0$, where $U_{eq}(r)$ is a vorticity at an equilibrium state. It is noted that a poloidal rotation is introduced through the vorticity $U_{eq}(r)$. In Eqs. (1) and (2), time is normalized to τ_{hp}, length to a, ψ to $B_0 a^2$, ϕ to $B_0 a^2/\tau_{hp}$ and U to B_0/τ_{hp}. Thus the velocity $\mathbf{v}_\perp$ is normalized with a/τ_{hp}.

Resistivity is introduced artificially in the vacuum region to use the pseudo-vacuum model.[18,19] Time evolution of the resistivity in Eq. (1) is solved here. The equation for resistivity is described as[20]

$$\frac{\partial\eta}{\partial t} = \frac{\partial\phi}{\partial r}\frac{1}{r}\frac{\partial\eta}{\partial\theta} - \frac{1}{r}\frac{\partial\phi}{\partial\theta}\frac{\partial\eta}{\partial r} + \kappa_\parallel\nabla_\parallel^2\eta + \kappa_\perp\nabla_\perp^2\eta + Q, \qquad (5)$$

where the parallel thermal transport coefficient of resistivity $\kappa_\parallel$ is normalized to R^2/τ_{hp} and the perpendicular one $\kappa_\perp$ to a^2/τ_{hp}. In the numerical calculations $\kappa_\parallel = 1$ and $\kappa_\perp = 10^{-5}$ are assumed. The source term Q is chosen to satisfy $\kappa_\perp\nabla_\perp^2\eta_{eq}(r) + Q = 0$, where $\eta_{eq}(r)$ is a resistivity at an equilibrium state.

The pseudo-vacuum region is surrounded by the resistive wall with a finite thickness. In the resistive wall, the velocity is zero and the resistivity is independent of time. However, the poloidal flux may change in this region. Thus, the diffusion equation of perturbed poloidal flux $\tilde\psi$

$$\frac{\partial\tilde\psi}{\partial t} = \eta_w\nabla_\perp^2\tilde\psi \qquad (6)$$

is solved in the resistive wall, where η_w is a resistivity of the resistive wall.

It is assumed that the outside of resistive wall is covered by a perfect conductor at $r_c = 2$ for simplicity. In this case, the main plasma is located in the region $r \leq 1$, the pseudo-vacuum in the region $1 < r < r_w$, and the resistive wall in the region $r_w \leq r \leq r_c$, where r_w is the boundary between the pseudo-vacuum and the resistive wall. The boundary conditions for the reduced MHD equations solving $\tilde\phi(r,\theta,\zeta,t)$, $\tilde\psi(r,\theta,\zeta,t)$ and $\tilde\eta(r,\theta,\zeta,t)$ are $\tilde\phi(r_w) = \tilde\eta(r_w) = 0$ at $r = r_w$ and $\tilde\psi(r_c) = 0$ at $r = r_c$. At $r = 0$ standard boundary conditions are employed.

The current profile at an equilibrium state is chosen as

$$J_{eq}(r) = (J_a - J_b)(1 - r^{3.5})^2 + J_b \qquad (7)$$

for $0 \leq r \leq 1$, and $J_{eq}(r) = J_b \ll J_a$ for $1 < r < r_c$. The resistivity profile is assumed to be proportional to $1/J_{eq}(r)$ for $r < r_w$, $\eta(r=0)$ and the resistivity in the pseudo-vacuum region η_v are set to be $\eta(r=0) = 10^{-5}$ and $\eta_v = 10^{-3}$, respectively. Resistivity of the resistive wall η_w is assumed to be
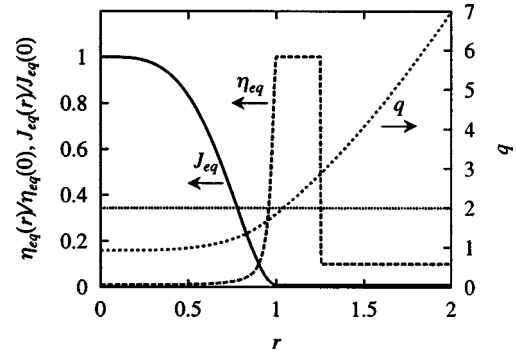

FIG. 1. Profiles of safety factor q, plasma current density J_{eq} and resistivity η_{eq} at equilibrium state.

$\eta_w = 10^{-4}$. The profiles of q, J_{eq} and η_{eq} are shown in Fig. 1, where q is a safety factor. In Fig. 1, $q_a = 1.85$ and $r_w = 1.2$ are assumed, where q_a is a safety factor at the plasma surface. The rational surface of $q=2$ is located at $r = r_s \simeq 1.04$ in the pseudo-vacuum region. For studying nonlinear RWMs, this configuration has been used.

Equations (1)–(5) are solved numerically for the cylindrical plasma shown in Fig. 1. In our numerical code, the radial derivates are replaced with standard difference approximations. the derivatives with respect to poloidal angle θ and the toroidal angle ζ are treated with Fourier-expansions. We also assume single helicity for studying the $(m,n) = (2,1)$ mode destabilized at the $q=2$ surface, since our interest is in the unstable low-m modes. The time advancement is made with a predictor-corrector method. A typical radial mesh number is 400 and 10 harmonics of the $(2,1)$ mode are solved in nonlinear calculations. These numbers are sufficient from the point of view of numerical accuracy.

III. NUMERICAL RESULTS

A. Nonlinear behavior of RWMs without a poloidal rotation

Figure 2 shows dependence of linear growth rate of the $(m,n) = (2,1)$ mode on the resistive wall position given by r_w. For obtaining linear growth rate in case of a perfect conducting wall, the boundary conditions are changed to standard ones, $\tilde\psi(r_w) = \tilde\phi(r_w) = \tilde\eta(r_w) = 0$ at $r = r_w$. When

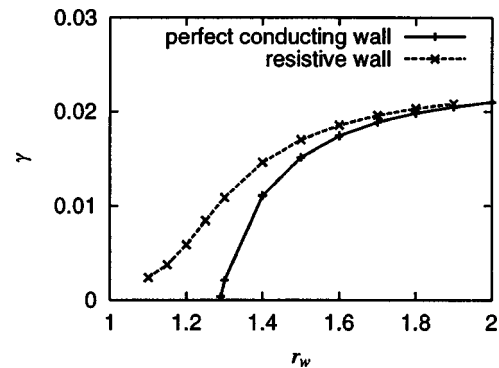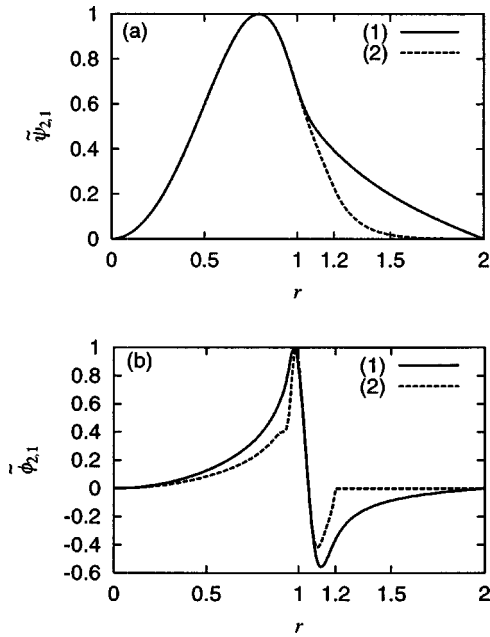FIG. 2. Dependence of linear growth rate γ of $(m,n) = (2,1)$ mode on wall position r_w.

FIG. 3. Linear eigenfunction of (a) $\tilde{\psi}_{2,1}$ and (b) $\tilde{\phi}_{2,1}$. Line (1) corresponds to the perfect conducting wall case. Line (2) corresponds to the case that the resistive wall is located at $r_w = 1.2$ and $\omega_{eq} = 0$ (no poloidal rotation).

the perfect conducting wall is located at $r \lesssim 1.27$ instead of the resistive wall, the ideal kink mode can be stabilized completely. When a resistive wall is assumed, RWMs become always unstable. Radial profile of linear eigen function of $\tilde{\psi}_{2,1}$ and $\tilde{\phi}_{2,1}$ for the case of $r_w = 1.2$ is shown in Fig. 3. For the resistive wall case, the magnetic flux diffuses into the wall clearly.

Time evolution of magnetic energy and kinetic energy without the poloidal rotation is shown in Fig. 4. Here, the resistive wall is assumed at $r_w = 1.2$. The perturbed magnetic energy saturates at $t = 2000$. The magnetic surfaces at $t = 2000$ are shown in Fig. 5(a). The contours of resistivity at $t = 2000$ are shown in Fig. 5(b). The cross-section of core plasma is deformed elliptically and magnetic islands are formed around the rational surface. Even when the region between the plasma surface and the resistive wall is replaced with a vacuum, $\tilde{\psi}$ has a finite perturbation at $r = r_s$ and vacuum magnetic islands are formed. The radial profile of $(m,n) = (0,0)$ component of perturbed resistivity $\tilde{\eta}_{0,0}$ is shown in Fig. 6. It is considered that the plasma confinement in the edge region become degraded due to the formation of island structure by the RWM.

B. Nonlinear behavior of RWMs with poloidal rotation

It is shown that RWMs can be stabilized by a large rigid poloidal rotation. Linear growth rates γ and mode frequency are plotted as a function of poloidal rotation frequency $\omega_{eq} = v_\theta / r$ in Fig. 7, where v_θ is a poloidal flow velocity proportional to r. For $r_w = 1.3$, the mode cannot be stabilized perfectly by the rigid poloidal rotation, because the ideal kink mode with $(m,n) = (2,1)$ becomes marginally unstable.

As shown in Fig. 7(b), the mode frequency is smaller than ω_{eq}, and the difference between ω_{eq} and the mode
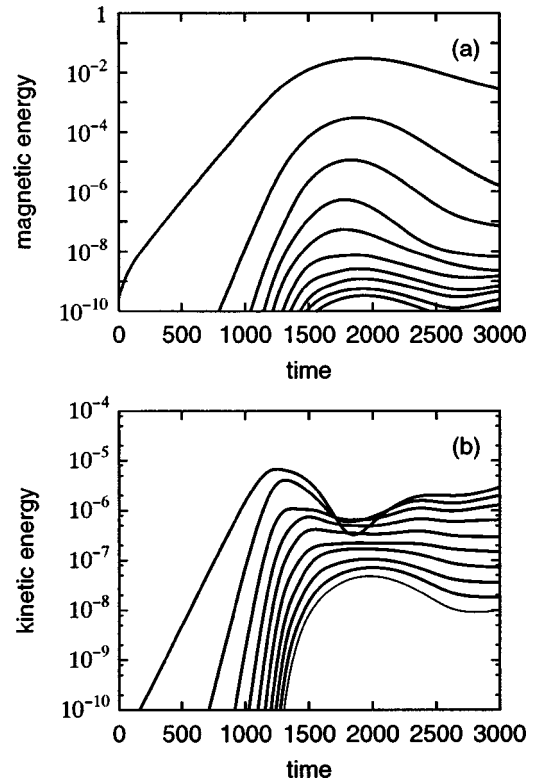

FIG. 4. Time evolution of (a) magnetic energy and (b) kinetic energy without a poloidal rotation. Resistive wall is assumed to be located at $r_w = 1.2$. Mode numbers for 10 lines in both figures are $(2,1),(4,2),(6,3),\ldots,(20,10)$ respectively from the top line.

frequency increase when r_w is decreased. This is a general behavior of mode frequency of RWM, when the resistive wall position is changed.[4,14] A significant effect of ω_{eq} on the RWM is the appearance of the phase shift δ depending on r as shown in Fig. 8(a). For understanding the stabilizing effect of poloidal rotation, it is useful to check positions satis-
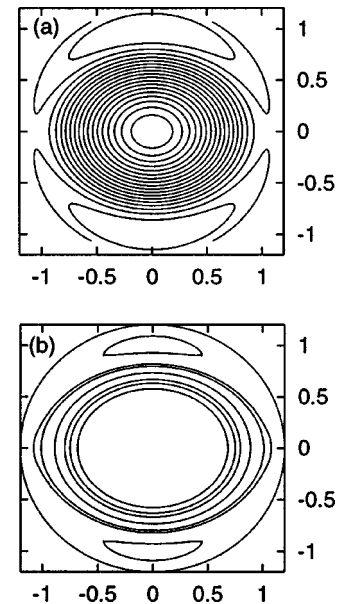

FIG. 5. (a) Magnetic surfaces, and (b) contours of resistivity at the saturation phase ($t = 2000$) corresponding to Fig. 4.
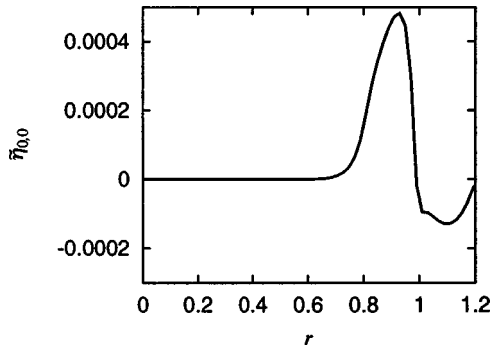
FIG. 6. Radial profile of $(m,n)=(0,0)$ component of perturbed resistivity $\tilde{\eta}_{0,0}$ at saturation phase ($t=2000$) corresponding to Fig. 4.

fying $\psi_{2,1}(r,\theta,0)=0$ in Fig. 8(b). When $\omega_{eq}=0$, $\psi_{2,1}(r,\theta,0)=0$ at $\theta=\rho/2$ or $3\pi/2$. However, for $\omega_{eq}\neq0$, the curve satisfying $2\theta-\delta(r)=\pi/2$ or $3\pi/2$ gives $\psi_{2,1}(r,\theta,0)=0$. According to linear calculations of RWM, $d\delta/dr$ becomes large with the increase of ω_{eq}. Thus, as shown in Fig. 8(b), $\psi_{2,1}(r,\theta,0)=0$ is satisfied on $r\simeq$ const surface roughly for a large ω_{eq} case. This situation is similar to the case with a perfectly conducting wall which stabilize kink modes easily.

Since our interest is in cases with r_w larger than 1.15–1.2, the stabilizing effect of poloidal rotation becomes dominant. However, when the resistive wall is close to the core plasma or $r_w<1.1$, the mode frequency becomes almost zero and destabilizing effect due to plasma rotation appears.[4,14] For such a case with $r_w<1.1$, the coupling of RWM to the other mode such as magnetosonic wave or shear Alfvén wave becomes essential to reduce the growth rate of RWM
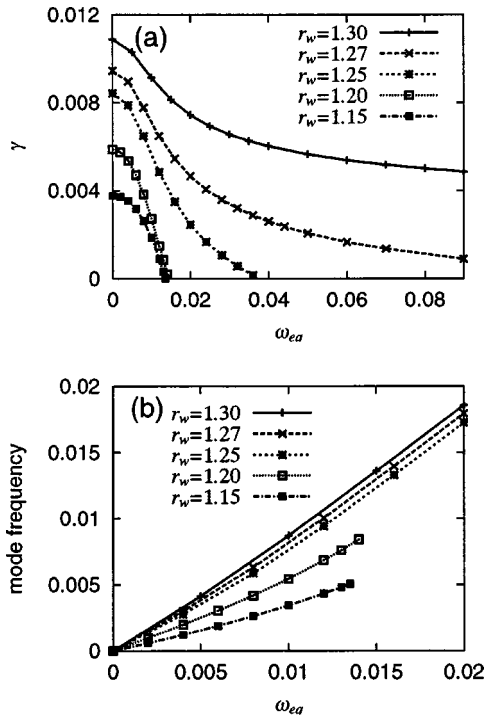

FIG. 7. Dependence of (a) linear growth rate γ and (b) mode frequency on poloidal rotation frequency ω_{eq} for various resistive wall positions.
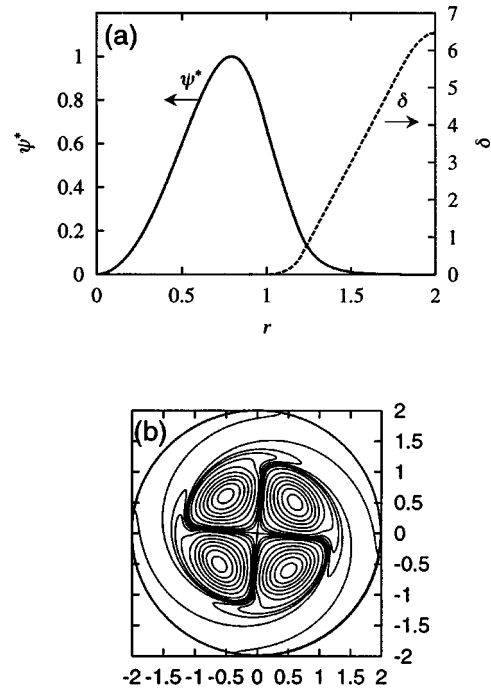

FIG. 8. Linear mode structures of RWM with $(m,n)=(2,1)$ mode described by $\psi_{2,1}(r,\theta,0)=\psi^*(r)\cos(2\theta-\delta(r))$ for $r_w=1.2$ and $\omega_{eq}=1.3\times10^{-2}$; (a) shows $\psi^*(r)$ and $\delta(r)$, and (b) shows contours of $\psi_{2,1}(r,\theta,0)$.

in the cylindrical geometry.[13,14] For a toroidal case, more efficient toroidal coupling to sidebands becomes possible.[10,11]

Time evolution of magnetic energy of the $(m,n)=(2,1)$ component for $r_w=1.27$ for various poloidal rotation frequencies is shown in Fig. 9. When a poloidal rotation is sufficiently large such as $\omega_{eq}\geq4\times10^{-2}$, the RWM saturates at a lower level than that in the case with $\omega_{eq}=0$. However, when the poloidal rotation velocity is small, the RWM saturates at the level comparable to that of $\omega_{eq}=0$ case. For $\omega_{eq}=3\times10^{-2}$, after the mode almost saturate at $t\simeq2500$ temporally, the mode grows again at $t\simeq3000$.

The difference of the saturation level is related to the change of poloidal rotation. Figure 10 shows time evolution of profile of poloidal rotation velocity, $v_\theta(r)=v_{eq}(r)+\tilde{v}_{0,0}(r)$, for (a) $\omega_{eq}=3\times10^{-2}$ and (b) $\omega_{eq}=4\times10^{-2}$, re-
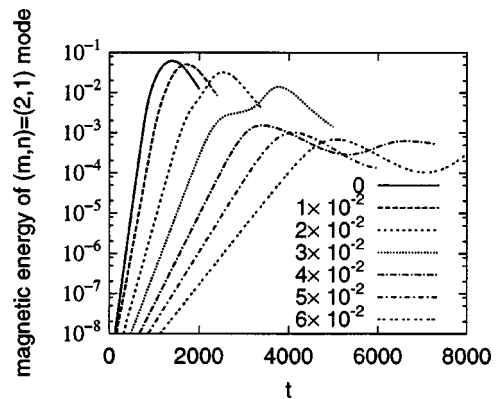

FIG. 9. Time evolution of magnetic energy of $(m,n)=(2,1)$ mode for $r_w=1.27$ for various poloidal rotation frequencies.

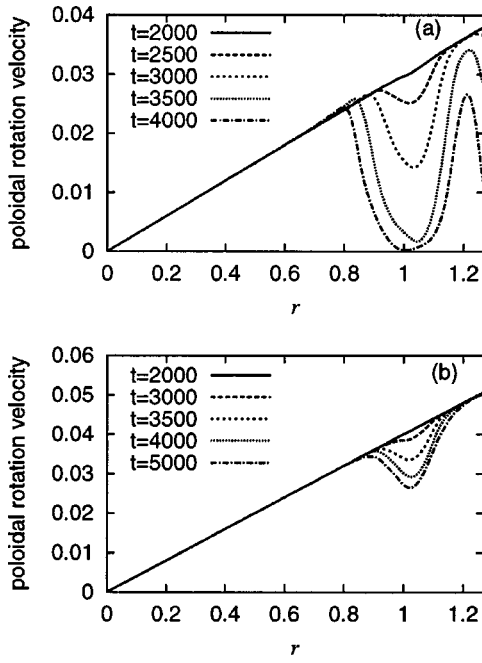FIG. 10. Time evolution of radial profile of poloidal rotation velocity for (a) $\omega_{eq}=3\times10^{-2}$ and (b) $\omega_{eq}=4\times10^{-2}$ corresponding to Fig. 9.

FIG. 12. Time evolution of radial profile of poloidal rotation velocity for $\omega_{eq}=1.3\times10^{-2}$ corresponding to Fig. 11.

spectively. For both cases, there is a slowdown of poloidal rotation velocity in the nonlinear phase. For $\omega_{eq}=3\times10^{-2}$, the poloidal rotation velocity begins to decrease at $t\simeq2500$ and it decreases to almost zero around the rational surface after $t\simeq3000$. Thus, after $t\simeq3000$ the stabilization effect of poloidal rotation becomes weak and the mode grows again. However, for $\omega_{eq}=4\times10^{-2}$, a substantial poloidal rotation velocity remains even in the nonlinear phase. Thus, the saturation level becomes low due to the stabilization effect of the poloidal rotation.

Figure 11 shows time evolution of magnetic energy of the $(m,n)=(2,1)$ component for $r_w=1.2$ which is chosen as an example of the case that the wall is close to the plasma surface. The linear growth rate for $r_w=1.2$ at $\omega_{eq}=1.3\times10^{-2}$ in Fig. 11 is smaller than that for $r_w=1.27$ at $\omega_{eq}=4\times10^{-2}$ in Fig. 9. However, in the case of $r_w=1.2$ at $\omega_{eq}=1.3\times10^{-2}$, the nonlinear growth rate is enhanced at t
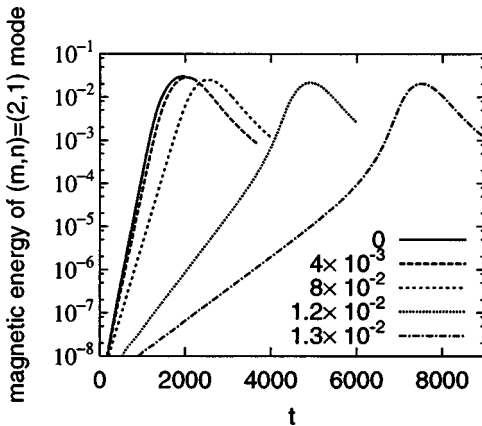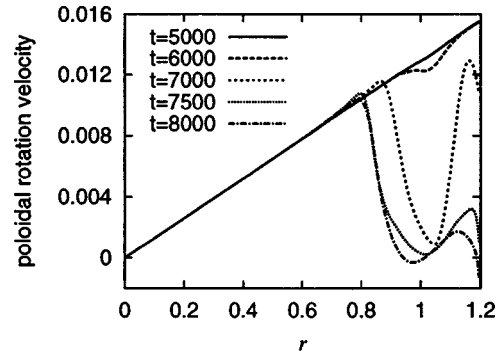
$\simeq6000$. In this case, the poloidal rotation velocity begins to decrease near the rational surface after $t=6000$ (see Fig. 12). As the poloidal rotation velocity decreases, the growth of RWM is enhanced. The increase of perturbation amplitude leads to further reduction of the poloidal rotation velocity. Finally, the poloidal rotation velocity become almost zero in the regions near the plasma surface and the resistive wall surface in Fig. 12. As shown in Fig. 11, the saturated amplitude in case of $\omega_{eq}\neq0$ becomes comparable to that for the $\omega_{eq}=0$ case even though linear growth rate is smaller than that for the $\omega_{eq}=0$ case.

Figure 13 shows dependence of the saturation level of magnetic energy of the $(m,n)=(2,1)$ component on the poloidal rotation frequency. When the distance between the plasma surface and the resistive wall surface becomes wider, the poloidal rotation velocity required to stabilize the RWM becomes larger. However, if the initial poloidal rotation velocity is large, the poloidal rotation survives in the nonlinear phase and the saturation level is much lower than that for the $\omega_{eq}=0$ case. When the resistive wall is very close to the plasma surface, the reduction of poloidal rotation is significant in the nonlinear phase. Then the resistive wall mode may grow up to the saturation level in the $\omega_{eq}=0$ case regardless of the value of the poloidal rotation frequency.

C. Mechanism of slowdown of poloidal rotation

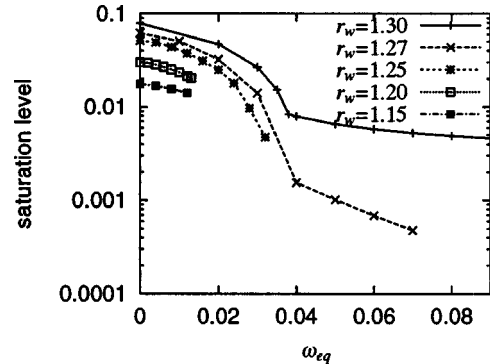The time evolution of averaged poloidal rotation velocity $\langle v_\theta \rangle$ is described by

FIG. 11. Time evolution of magnetic energy of $(m,n)=(2,1)$ mode for $r_w=1.2$ for various poloidal rotation frequencies.

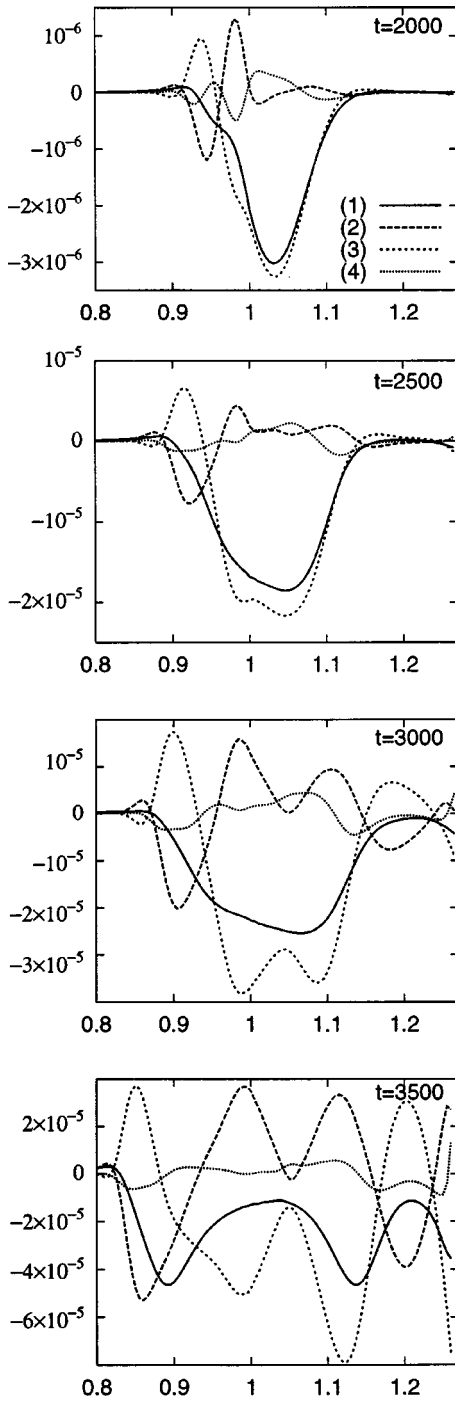FIG. 13. Dependence of maximum magnetic energy of $(m,n)=(2,1)$ mode on the initial poloidal rotation frequency.

FIG. 14. Time evolution of radial profile of each term in Eq. (8) for r_w = 1.27 at $\omega_{eq} = 3 \times 10^{-2}$. Here curve (1) denotes left-hand side of Eq. (8), curve (2) denotes the first term of right-hand side of Eq. (8) corresponding to Reynolds stress, curve (3) denotes the second term of RHS of Eq. (8) corresponding to Maxwell stress, and curve (4) denotes the third term of RHS of Eq. (8) corresponding to viscous damping.

FIG. 15. Time evolution of radial profile of each terms in Eq. (8) for r_w = 1.27 at $\omega_{eq} = 4 \times 10^{-2}$. Here curves (1), (2), (3), (4) denote the same term in Eq. (8), respectively, as shown in Fig. 14.

$$\frac{\partial \langle v_\theta \rangle}{\partial t} = -\frac{1}{r^2} \frac{\partial}{\partial r} r^2 \langle \tilde{v}_r \tilde{v}_\theta \rangle + \frac{1}{r^2} \frac{\partial}{\partial r} r^2 \langle \tilde{B}_r \tilde{B}_\theta \rangle - \nu \frac{d \tilde{U}_0}{dr},$$
$$(8)$$

where $\langle f \rangle = \int_0^{2\pi} f \, d\theta d\zeta / 4\pi^2$ and $\tilde{U}_0$ is $(m,n) = (0,0)$ component of perturbed vorticity. Equation (8) is obtained by taking the average of Eq. (2) over θ and ζ. In order to study the mechanism of generation or decay of the poloidal rotation,
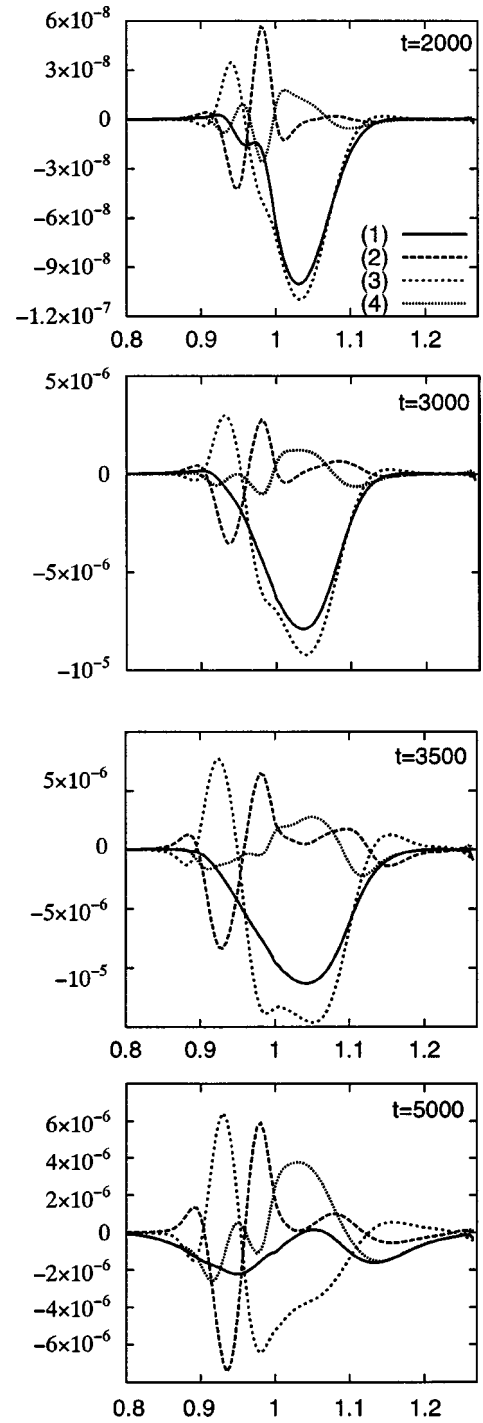
the three terms in the right hand side of Eq. (8) are treated separately. Time evolution of radial profile of each term in Eq. (8) for $r_w = 1.27$ at $\omega_{eq} = 3 \times 10^{-2}$ and for $r_w = 1.27$ at $\omega_{eq} = 4 \times 10^{-2}$ are shown in Fig. 14 and Fig. 15, respectively. Generally the second term or Maxwell stress is dominant in the RHS of Eq. (8). The Maxwell stress largest in the vicinity of the rational surface becomes a damping force. The electrostatic Reynolds stress corresponding to the first term in the RHS of Eq. (8) has a tendency to generate the poloidal
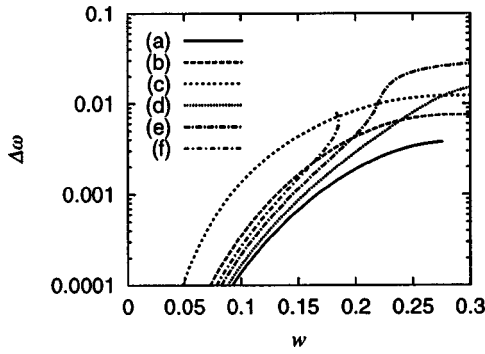
FIG. 16. Island width w vs $\Delta\omega = \omega_{eq} - \omega(t)$ at $r = r_s$. (a) $r_w = 1.2$, $\omega_{eq} = 4 \times 10^{-3}$, (b) $r_w = 1.2$, $\omega_{eq} = 8 \times 10^{-3}$, (c) $r_w = 1.2$, $\omega_{eq} = 1.3 \times 10^{-2}$, (d) $r_w = 1.27$, $\omega_{eq} = 2 \times 10^{-2}$, (e) $r_w = 1.27$, $\omega_{eq} = 3 \times 10^{-2}$, and (f) $r_w = 1.27$, $\omega_{eq} = 4 \times 10^{-2}$.

FIG. 18. Time evolution of a torque acting inside the plasma (continuous line) and that inside the wall (dotted line) for $r_w = 1.27$ at $\omega_{eq} = 3 \times 10^{-2}$.

flow. However its contribution is weak for RWMs. Although the viscosity effect given by the third term in the RHS of Eq. (8) works to generate the poloidal flow near the rational surface, its effect is not large. For $\omega_{eq} = 4 \times 10^{-2}$, the mode saturate at $\simeq 3400$ as shown in Fig. 9, however, the poloidal rotation velocity remains at this time [see Fig. 10(b)]. Since the perturbed magnetic energy of $(m,n) = (2,1)$ mode decays after $t \simeq 3400$ as shown in Fig. 9, the Maxwell stress also decreases after the saturation. Thus, the reduction of poloidal rotation also become small, and the finite poloidal rotation velocity is kept in the nonlinear phase.

Figure 16 shows a relation between the magnetic island width (full width) due to the RWM of $(m,n) = (2,1)$ mode and $\Delta\omega = \omega_{eq} - \omega(t)$ at the rational surface. Here $\omega(t)$ denotes a time dependent poloidal rotation frequency of the rational surface, and the magnetic island width also depends on time. The poloidal rotation velocity begins to decrease at smaller island width, when the initial poloidal rotation velocity becomes larger. When the resistive wall is close to the plasma surface ($r_w = 1.2$), the poloidal rotation velocity begins to decrease at smaller island width than the case for $r_w = 1.27$. The Maxwell stress is larger for $r_w = 1.2$ than for $r_2 = 1.27$ at the same island width as shown in Fig. 17. It is noted that the Maxwell stress becomes maximum for a specific magnetic island width. When the resistive wall is close
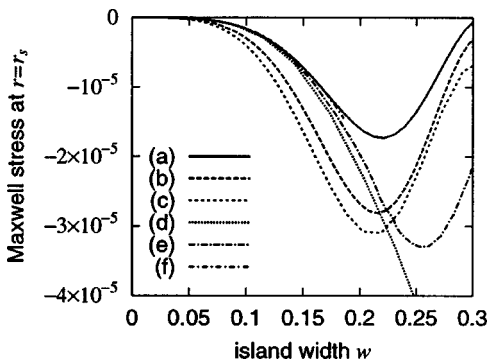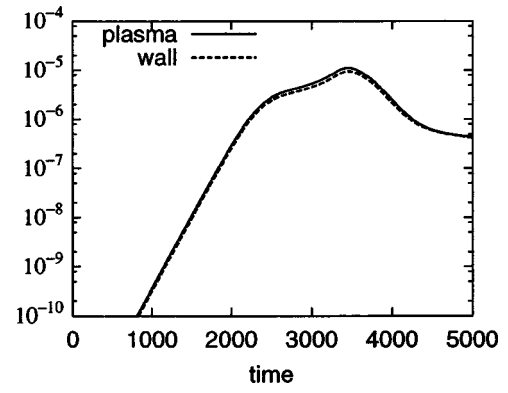
to the plasma surface and the initial poloidal rotation velocity is large, the nonlinear RWM is affected by the large Maxwell stress at $r \simeq r_s$. The poloidal rotation velocity is also affected by the Maxwell stress in case of a smaller linear growth rate, since the magnetic island keeps the width corresponding to the maximum Maxwell stress for a longer time. Thus, the poloidal rotation velocity decreases significantly for r_w
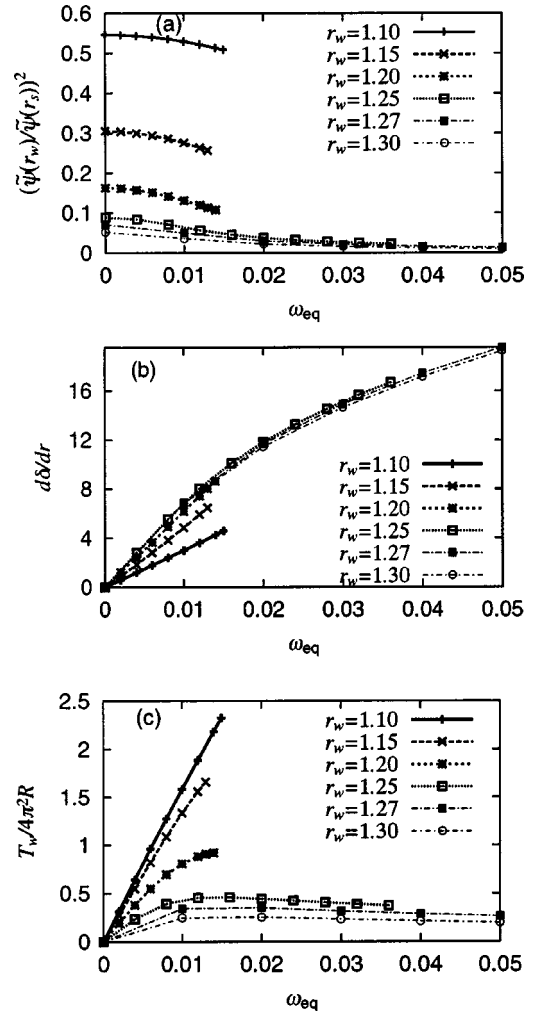
FIG. 19. Dependence of (a) $(\tilde{\psi}(r_w)/\tilde{\omega}(r_s))^2$, (b) $d\delta/dr$, and (c) T_w on initial poloidal rotation frequency in linear phase.

FIG. 17. Island width w vs Maxwell stress at $r = r_s$, (a) $r_w = 1.2$, $\omega_{eq} = 4 \times 10^{-3}$, (b) $r_w = 1.2$, $\omega_{eq} = 8 \times 10^{-3}$, (c) $r_w = 1.2$, $\omega_{eq} = 1.3 \times 10^{-2}$, (d) $r_w = 1.27$, $\omega_{eq} = 2 \times 10^{-2}$, (e) $r_w = 1.27$, $\omega_{eq} = 3 \times 10^{-2}$, and (f) $r_w = 1.27$, $\omega_{eq} = 4 \times 10^{-2}$.

$=1.2$ at $\omega_{eq}=1.3\times10^{-2}$. In this case, the poloidal rotation begins to decrease before the mode saturates as shown in Fig. 11 and Fig. 12.

Figure 18 shows time evolution of a rotational torque T_p acting inside the plasma and magnetic torque T_w acting inside the resistive wall for $r_w=1.27$ at $\omega_{eq}=3\times10^{-2}$. Here T_p and T_w are defined as

$$T_p=\int_{\text{plasma}}\left|\frac{\partial\langle v_\theta\rangle}{\partial t}\right|r\,dV=4\pi^2R\int_0^{r_w}\left|\frac{\partial\langle v_\theta\rangle}{\partial t}\right|r\,dr, \quad (9)$$

$$T_w=\int_{\text{wall}}\frac{1}{r^2}\frac{\partial}{\partial r}r^2\langle\tilde{B}_r\tilde{B}_\theta\rangle r\,dV$$

$$=4\pi^2R\int_{r_w}^2\frac{1}{r^2}\frac{\partial}{\partial r}r^2\langle\tilde{B}_r\tilde{B}_\theta\rangle r\,dr. \quad (10)$$

The contribution from the Reynolds stress and the viscosity to T_p is negligible. Here T_p is almost equal to T_w, which means that the poloidal rotation velocity decreases due to the magnetic torque inside the resistive wall.

It is noted that the perturbation $\tilde{\psi}(r,\theta,\zeta)$ is written as $\tilde{\psi}(r,\theta,\zeta)=\Sigma_{m,n}\tilde{\psi}_{m,n}(r)\cos(m\theta+n\zeta-\delta_{m,n})$. Since the contribution of the $(m,n)=(2,1)$ component to T_w is dominant as shown in Fig. 8, other higher harmonics may be negligible. Then T_w is written as

$$T_w/4\pi^2R=\int_{r_w}^2\frac{m}{2r^2}\frac{d}{dr}\left(r\tilde{\psi}_{m,n}^2\frac{d\delta_{m,n}}{dr}\right)r^2dr$$

$$=\frac{m}{2}\left(r\tilde{\psi}_{m,n}^2\frac{d\delta_{m,n}}{dr}\right)_{r=r_w} \quad (11)$$

by using $\tilde{\psi}_{m,n}$ and $d\delta_{m,n}/dr$ at the boundary between the resistive wall and the pseudo-vacuum.[15] Figure 19 shows (a) $(\tilde{\psi}_{2,1}(r_w)/\tilde{\psi}_{2,1}(r_s))^2$, (b) $d\delta_{2,1}/dr$, and (c) T_w in the linear phase, respectively, as a function of ω_{eq}. Since $\tilde{\psi}_{2,1}$ decreases monotonically for $r>r_s$, $(\tilde{\psi}_{2,1}(r_w)/\tilde{\psi}_{2,1}(r_s))^2$ become large as the position of resistive wall becomes close to the plasma surface. Also, $d\delta_{2,1}/dr$ becomes large for the large ω_{eq} case [see Fig. 19(b)], and T_w increases when the resistive wall becomes closer to the plasma surface [see Fig. 19(c)]. Thus, when the resistive wall becomes close to the plasma surface, the Maxwell stress increases.

IV. SUMMARY

Nonlinear behavior of the RWM of $(m,n)=(2,1)$ mode has been clarified with the reduced MHD model. Here the vacuum is treated with the pseudo-vacuum model and the poloidal rigid rotation is assumed as the initial condition.

When a resistive wall is placed close to the plasma surface such as $r_w\lesssim1,2$, the reduction of initially imposed poloidal rotation is significant and, the poloidal velocity almost disappears near the resonant surface. Then the RWM grows up to the saturation level in the case of $\omega_{eq}=0$. Thus the saturation level becomes independent of the initial poloidal rotation. When the distance between the plasma surface and the resistive wall becomes wider such as $r_w\simeq1.27$, the poloidal rotation velocity required to stabilize the linear RWM increases. However, if the poloidal rotation frequency is sufficiently large, the poloidal rotation survives even in the nonlinear phase. In this case, the saturation level decreases due to the increase of poloidal rotation. Finally it has been shown that the poloidal rotation is damped by the Maxwell stress dominantly. Here the magnetic torque is calculated for explaining this result. Also the dependence of Maxwell stress on the magnetic island width is shown.

[1] F. Troyon, R. Gruber, H. Saurenmann, S. Semenzato, and S. Succi, Plasma Phys. Controlled Fusion **26**, 209 (1984).
[2] J. P. Freidberg, *Ideal Magnetohydrodynamics* (Plenum, New York, 1987).
[3] V. D. Shafranov, Sov. Phys. Tech. Phys. **15**, 175 (1970).
[4] J. M. Finn, Phys. Plasmas **2**, 198 (1995).
[5] T. S. Taylor, E. J. Strait, L. L. Lao, M. Mauel, A. D. Turnbull, K. H. Burrell, M. S. Chu, J. R. Ferron, R. J. Groebner, R. J. La Haye, B. W. Rice, R. T. Snider, S. J. Thompson, D. Wròblewski, and D. J. Lightly, Phys. Plasmas **2**, 2390 (1995).
[6] M. Okabayashi, N. Pomphrey, J. Manickam, D. J. Ward, R. E. Bell, R. E. Hatcher, R. Kaita, S. M. Kaye, H. W. Kugel, B. Leblanc, F. M. Levinton, D. W. Roberts, S. Sesnic, Y. Sun, and H. Takahashi, Nucl. Fusion **36**, 1167 (1996).
[7] A. M. Garofalo, A. D. Turnbull, E. J. Strait, M. E. Austin, J. Bialek, M. S. Chu, E. Fredrickson, R. J. La Haye, G. A. Navratil, L. L. Lao, E. A. Lazarus, M. Okabayashi, B. W. Rice, S. A. Sabbagh, J. T. Scoville, T. S. Taylor, M. L. Walker, and The DII-D Team, Phys. Plasmas **6**, 1893 (1999).
[8] A. H. Boozer, Phys. Plasmas **5**, 3350 (1998).
[9] M. Okabayashi, J. Bialek, M. S. Chance, M. S. Chu, E. D. Fredrickson, A. M. Garofalo, M. Gryaznevich, R. E. Hatcher, T. H. Jensen, L. C. Johnson, R. J. La Haye, E. A. Lazarus, M. A. Makowski, J. Manickam, G. A. Navratil, J. T. Scoville, E. J. Strait, A. D. Turnbull, M. L. Walker, and the DII-D Team, Phys. Plasmas **8**, 2071 (2001).
[10] A. Bondeson and D. J. Ward, Phys. Rev. Lett. **72**, 2709 (1994).
[11] R. Betti and J. P. Freidberg, Phys. Rev. Lett. **74**, 2949 (1995).
[12] R. Fitzpatrick and A. Y. Aydemir, Nucl. Fusion **36**, 11 (1996).
[13] C. G. Gimblett, R. J. Hasite, R. A. M. Van der Linden, and J. A. Wesson, Phys. Plasmas **3**, 3619 (1996).
[14] A. Yoshioka, T. Tatsumo, and M. Wakatani, J. Phys. Soc. Jpn. **67**, 3794 (1998).
[15] M. F. F. Nave and J. A. Wesson, Nucl. Fusion **30**, 2575 (1990).
[16] B. B. Kadomtsev and O. P. Pogutse, Sov. Phys. JETP **38**, 283 (1974).
[17] H. R. Strauss, Phys. Fluids **19**, 134 (1976).
[18] G. Kurita, M. Azumi, T. Takizuka, T. Tuda, T. Tsunematsu, Y. Tanaka, and T. Takeda, Nucl. Fusion **26**, 449 (1986).
[19] Yu. N. Dnestrovskii, D. P. Kostomarov, A. M. Popov, and É. A. Shagirov, Sov. J. Plasma Phys. **11**, 616 (1985).
[20] B. A. Carreras, P. W. Gaffney, H. R. Hicks, and J. D. Callan, Phys. Plasmas **25**, 1231 (1982).